Bachelor's Thesis

THz vortex beam generation with 3D printed spiral phase plates

conducted at

Institute for Solid State Physics

Vienna University of Technology

Wiedner Hauptstrasse 8-10

1040 Wien

by

Blanka Bekecs

51867965

Supervisors:

Dr. Evan Constable

Prof. Andrei Pimenov

Vienna, 27.05.2024

_____

Name

Abstract

THz vortex beam generation with 3D printed spiral phase plates

This thesis explores the generation of Terahertz vortex beams using 3D printed spiral phase plates and their potential application in spectroscopy. Starting with theoretical foundations touching upon Terahertz radiation, polarized light, optical vortices, and spiral phase plates, we delve into the design and fabrication process of spiral phase plates, ensuring alignment with 3D printing parameters. Experimentation involved five setups aimed at shedding light on the influence of spiral phase plates on light wavefronts, how they propagate through optical elements and the feasibility of utilizing helical beams for spectroscopic purposes. Results demonstrate successful generation and control of helical beams, validating the effectiveness of spiral phase plates, especially in spectroscopically relevant setups. Notably, we achieved the reversal of the vortex effect using a second spiral phase plate, transforming the helical beam back into a planar wavefront. Challenges such as non-planar wavefronts were addressed, and future research avenues identified such as optimizing optical alignment and exploring higher-order spiral phase plates for enhanced control of light waves. This work contributes to advancing knowledge in optical manipulation and lays groundwork for practical applications in communication, imaging, and beyond.

Table of Contents

1. Introduction

In recent years, there has been a growing interest in the generation of Terahertz vortex beams and their potential applications in various fields such as imaging [1], wireless communication [2], nondistructive testing [3] and spectroscopy [1]. The Terahertz region of the electromagnetic spectrum, which lies between the microwave and infrared frequencies, offers unique properties that make it attractive for a wide range of applications. One of the key properties that make Terahertz radiation intriguing is its ability to penetrate non-conductive materials, such as plastics, clothing, and paper [4], while being safe for biological tissues [5]. More about the THz range is explained in subsection 2.1. However, the generation of Terahertz vortex beams has been relatively unexplored compared to other frequency bands.

The focus of this thesis was to create vortex beams using radiation in the THz range with a 3D-printed spiral phase plate (SPP). By designing and fabricating 3D printed SPPs, we aimed to demonstrate the basic functionalities of Terahertz orbital angular momentum. One advantage of 3D printing is its capability to produce complex and customized structures with high precision and resolution, making it suitable for fabricating SPPs for Terahertz vortex beam generation. This technology provides an efficient and low-cost method for wavefront modulation in the THz range.

The thesis begins with an introduction to THz radiation and the concept of orbital angular momentum in electromagnetic radiation. It explains the use of SPPs in our experiment and their manufacturing through 3D printing. The subsequent sections detail the experimental process, including the setup construction and design considerations for the SPP. Finally, the results are presented, analysed, and implications for future research in this field are discussed.

2. Theoretical background

2.1. THz radiation

Terahertz radiation is a portion of the electromagnetic spectrum with wavelengths that span from 100 mm to 1 mm. Positioned between infrared and microwave radiation, it possesses similar characteristics to its neighbouring regions. Extensive research has been conducted on both infrared and microwave radiations, leading to their integration into conventional electronic devices.

Compared to microwave radiation, THz waves exhibit less scattering and greater penetration depth. This property enables them to offer superior spatial resolution for imaging purposes [1].

The broad range of applications related to THz radiation has captivated researchers in diverse fields such as biomedicine, condensed matter physics, imaging technology, security measures and communication systems [2]. Furthermore, due to its strong absorption capabilities within this range of frequencies, THz radiation can exert notable effects on biological structures like DNA molecules and proteins by influencing their structure, functionality, and dynamics. These

unique properties of Terahertz radiation make it an attractive choice for various applications, including non-destructive testing and diagnostics, thermal imaging, and spectroscopy [3].

2.2. Polarization of light

Polarization refers to the confinement of the electric or magnetic field vector to a specific shape perpendicular to the direction of propagation for electromagnetic radiation (light).

Light can be represented mathematically (in the classic interpretation) as a solution of the electromagnetic wave equation. One such solution of that is a plane wave, given by

$$\vec{E} = \vec{E}_0 \, e^{i(\vec{k}\cdot\vec{r} - \omega t)},$$

where $\vec{E}_0$ denotes the complex amplitude of the wave, $\vec{k}$ is the wave number, ω the angular frequency, and t is time. The angular frequency is related to the wave number by $\omega = ck$ [7]. We choose z as the propagation direction.

Since $\vec{E}_0$ is perpendicular to $\vec{k}$, we can also write,

$$\vec{E}_0 = \begin{pmatrix} E_x \\ E_y \\ 0 \end{pmatrix} \text{ [7].}$$

Both E_x and E_y have a phase ϕ and a magnitude $|E|$, which we can formulate as

$$E_x = |E_x| \, e^{-i\phi_x} \;\; and \;\; E_y = \left|E_y\right| e^{-i\phi_y}.$$

These phases change over space and time, but their difference $\phi = \phi_x - \phi_y$ stays unaffected. Various techniques exist for polarizing light, including transmission, reflection, refraction, and scattering. Optical components such as polarizing beam splitters and half- and quarter-wave plates can also be used.

2.3. Linear polarization

A wave is linearly polarized when there is no phase difference ($\phi = 0$) between the phases of E_x and E_y. For the sake of simplicity, we assume that $E_y = 0$ and $E_x \neq 0$, and get,

$$\vec{E} = E_0 \hat{x} \, e^{i(kz - \omega t)},$$

which corresponds to a linear polarization in the x-direction. By setting that $E_x = 0$ and $E_y \neq 0$ we will obtain the linear polarization in the y-direction. As we are only interested in the real part of the solution the electric field vector of the linearly polarized electromagnetic wave will be

$$Re\left[\vec{E}\right] = \begin{pmatrix} E_0 \cos\,(kz - \omega t) \\ 0 \\ 0 \end{pmatrix}.$$

We can see that the real part of the wave is not dependent on x and y, which means that the wave is planar, and only the magnitude of the electric field varies in z and t [7].

Linearly polarized electromagnetic waves carry a linear momentum of,

$$\vec{p} = \hbar\vec{k} = \frac{\varepsilon}{c}\vec{k},$$

per photon. Here ε represents the energy of a photon, c the speed of light in vacuum, and $\vec{k}$ the propagation vector. The intensity of a monochromatic wave travelling in the z direction can be written as,

$$\vec{P} = c\varepsilon_0 E^2 \hat{z} = c\varepsilon_0 E_0^2 cos^2(kz - \omega t)\hat{z}$$ [7].

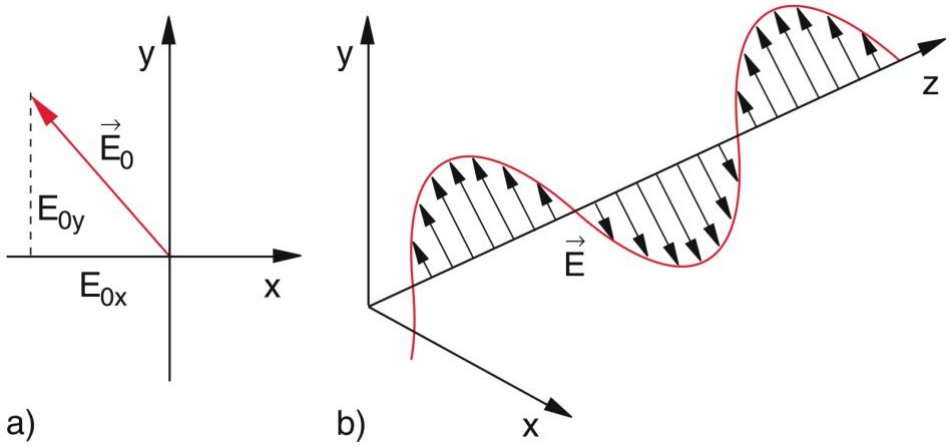

Figure 1: Representation of linearly polarized light. a) direction of E on the x-y plane. b) visual representation of the E-field in 3 dimensions [5]

2.4. Circular polarization

An electromagnetic wave can be circularly polarized when the x and y components of the electric field have a phase difference of $\phi = \pi/2$. In this case we can write the total field as,

$$\overrightarrow{E_0} = \begin{pmatrix} E_0 \\ E_0 e^{i\pi/2} \\ 0 \end{pmatrix} = \begin{pmatrix} E_0 \\ iE_0 \\ 0 \end{pmatrix}$$ [7].

Looking at the real part of the electric field vector again we obtain,

$$Re[\vec{E}] = \begin{pmatrix} E_0 \cos(kz - \omega t) \\ -E_0 \sin(kz - \omega t) \\ 0 \end{pmatrix},$$

which corresponds to a left-handed circular polarization. We can also see that for $\phi = -\pi/2$ we get right-handed circular polarization [7].

When combining left- and right-handed circular polarization we get a linearly polarized wave. When adding the 2 together,

$$\overrightarrow{E_0} = \begin{pmatrix} E_0 \\ iE_0 \\ 0 \end{pmatrix} + \begin{pmatrix} E_0 \\ -iE_0 \\ 0 \end{pmatrix} = \begin{pmatrix} 2E_0 \\ 0 \\ 0 \end{pmatrix},$$

the wave becomes polarized in the x direction, and when subtracting the right-handed wave from the left-handed wave,

$$\overrightarrow{E_0} = \begin{pmatrix} E_0 \\ iE_0 \\ 0 \end{pmatrix} - \begin{pmatrix} E_0 \\ -iE_0 \\ 0 \end{pmatrix} = \begin{pmatrix} 0 \\ 2iE_0 \\ 0 \end{pmatrix},$$

It becomes linearly polarized in the y direction.

Here we can see that circular and linear polarization are not linearly independent, therefore any polarization can be written as a linear combination of left- and right-handed polarization.

A circularly polarized beam also carries an angular momentum of $\pm e_0 \left|\vec{E}\right|^2$ (the positive sign for right-handed, and the negative sign for left-handed polarization). It also has an angular momentum density $\vec{J} = \vec{r} \times \vec{p}$, which we can see as the cross product of the radius vector $\vec{r}(r, 0, z)$ and the linear momentum density [7].

Unlike circularly polarized beams, linearly polarized ones do not carry angular momentum. This is because of the positive and negative signs in the linear combination cancel each other out.

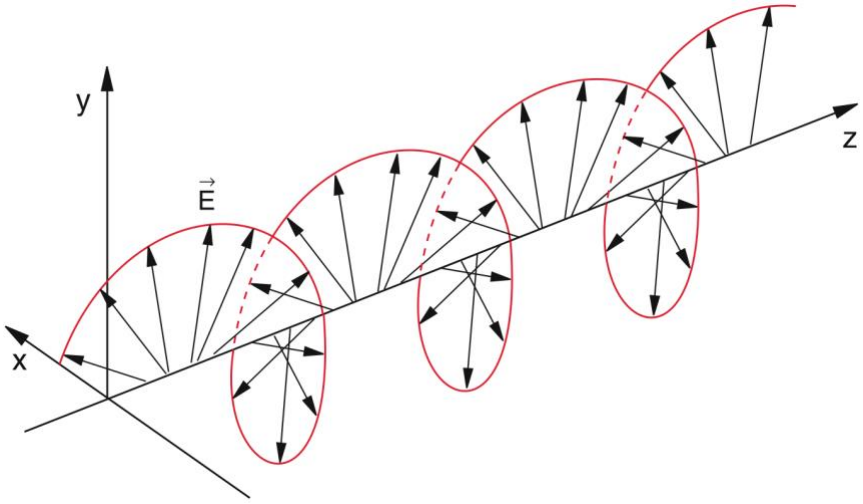

Figure 2: Visual representation of left circular polarization of an electromagnetic wave in 3 dimensions [5]

2.5. Optical vortices

The investigation of optical vortices has been conducted within the theoretical framework of Maxwell-Bloch theory, which encompasses the interaction between a 2-state quantum system and an optical resonator's electromagnetic mode. The Maxwell-Bloch equations can be derived from cavity quantum electrodynamics. In 1989, researchers discovered a vortex solution to these equations that exhibited stationary characteristics, with zero electric fields observed at these fixed locations. Consequently, it is possible to describe spiral waves revolving around the points where the electric field becomes singular, indicating a phase singularity in the electric field [6].

An optical vortex is a light beam that propagates with a singularity in phase $e^{il\varphi}$, around the axis. Here, φ represents the azimuthal angle in the transverse plane, and l denotes the topological charge resulting from its helicoidal spatial wavefront encircling the phase singularity [7].

2.6. Orbital angular momentum

Light beams that possess an azimuthal phase dependence of $e^{il\varphi}$ carry what is known as orbital angular momentum (OAM). This refers to the component of angular momentum that aligns with the direction in which the beam propagates, denoted as z. To have any form of angular momentum along this axis, there needs to be a presence of linear momentum components within the x-y plane, effectively creating transverse momenta for the light beam. The density of this angular momentum, represented by j, can be related to the density of linear momenta $p = \epsilon_0 E \times B$ through $j = r \times p$ where ϵ_0 denotes dielectric permittivity and × symbolizes the cross product between electric field (E) and magnetic field (B). For an angular momentum to be present in the z-direction, the electric and/or magnetic field of a transverse plane wave must also have a component in that same direction. This is because the linear momentum of the wave is aligned with its propagation direction, z [8].

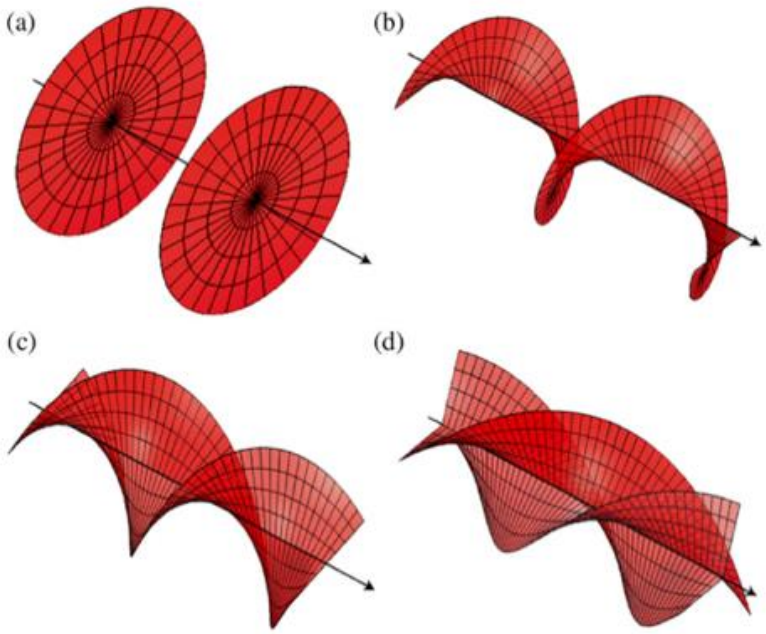

Figure 3: Helical phase fronts for different l-s
(a) l = 0 (planar wave), (b) l = 1, (c) l = 2 and (d) l = 3 [8]

An illustration of a light beam carrying orbital angular momentum can be seen in Fig. 3, where the phase in the transverse plane is given by,

$$\theta(r, \theta) = e^{il\varphi}.$$

In this case, θ represents the angular coordinate and l can take on any integer value (positive or negative). The beams exhibit helical phase fronts with intertwined helices, and their handedness is determined by the magnitude and sign of l respectively. It should be noted that an electromagnetic field perpendicular to these phase fronts will have axial components. Furthermore, the Poynting vector - which aligns parallel to the surface normal of the phase front at all times - possesses an azimuthal component around the light beam axis resulting in an angular momentum along that same axis [8].

It is well established that both the orbital angular momentum and spin angular momentum of a light beam are quantized in units of $\hbar$. This quantization remains distinct for most scenarios, whether approached through geometric principles or derived from Maxwell's

equations. Both concepts serve as valuable tools to analyse experimental situations in experiments [8].

There are multiple methods for generating THz vortex beams that can be grouped into 2 main categories. The first category includes the use of wavefront modulation techniques such as vortex plates. This includes, for example, SPPs (as was used in our experiment, with more details described in subsection 2.7.), THz q-plates, achromatic polarisation elements, diffractive optical elements, metasurfaces, and THz liquid crystal forked polarisation gratings. Another approach in this category utilizes THz hologram technology. The second category involves directly exciting the helicity of the THz vortex beam through techniques like optical rectification, difference-frequency generation, or laser plasma techniques [9].

2.7. Spiral phase plates

SPPs are optical components that manipulate the properties of waves by introducing a phase delay that varies with the azimuth angle. This is achieved by varying the thickness of the plate radially. The magnitude of this variation can be determined using the formula $h = l\,\lambda/\Delta n$, where h is the step height, l represents how much the topological charge changes, λ is the wavelength of light, and Δn is the difference in refractive index between the material the SPP is constructed from, and its surrounding medium. The total phase delay around the centre of the SPP is quantized and takes on integer multiples of 2π (expressed as $2\pi l$). The transmission function for an SPP can be defined as,

$$u(r,\theta) = circ\left(\frac{r}{R}\right)\exp\left(il\theta\right),$$

where r and θ denote radial and azimuthal coordinates respectively, R represents the effective aperture size of the SPP, and i denotes the imaginary unit [9].

One method for generating a beam with a helical phase is by passing a plane wave through a SPP, as depicted in Fig. 2. This SPP serves to demonstrate how the resulting beam carries orbital angular momentum and how this property is transferred from the optical component to the light. Consider the scenario where a beam of incident light strikes the flat surface of the phase plate at a perpendicular angle. It can be observed that upon exiting the helical face, the ray is refracted in an azimuthal direction. This leads to an increase in the angular momentum along the axis of the beam, as expressed by its linear momentum with respect to a radial vector [8].

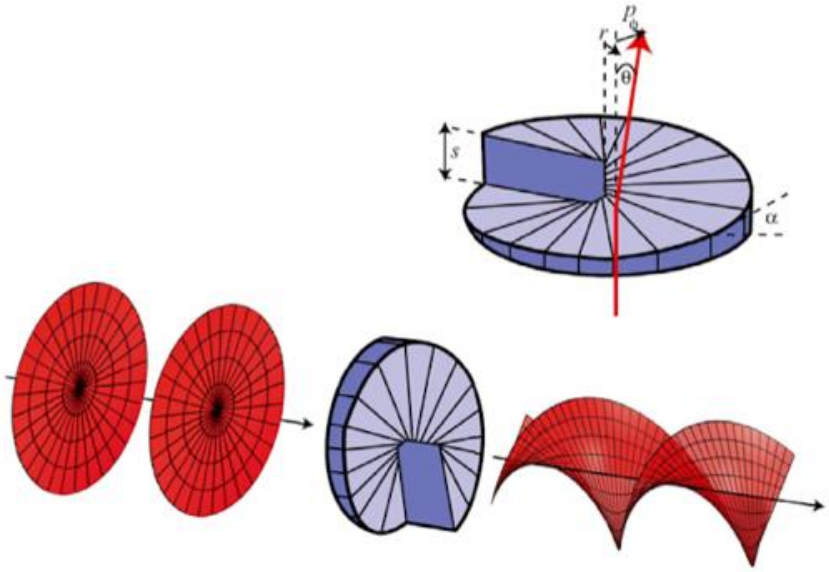

Figure 4: Generation of a helically phased beam from l = 0 to l = 2 [8]

Various materials such as Tsurupica olefin polymer, polylactic acid (PLA) medium, Teflon, and polypropylene-like materials can be used to fabricate SPPs. [9]

2.8. 3D printing technology

Additive manufacturing, also known as 3D printing, refers to the process of constructing a three-dimensional object using a digital 3D model or Computer Aided Design (CAD). This innovative technique involves assembling materials together in layers, often through methods like fusing polymers, liquids, or powder grains. The precise control over deposition, joining, and solidification is achieved by computer systems. Additive manufacturing offers several notable benefits such as the ability to create intricate designs freely and customize products on a large scale. Moreover, it reduces waste generation and facilitates rapid prototyping. This technology has revolutionized various industries by enabling the construction of complex structures with high efficiency [10].

In recent years, there has been a significant development in the availability of commercial high-quality 3D printing. This advancement allows for the cost-effective production of various components with intricate geometries. The effectiveness of 3D printing as a method for producing specialized elements, such as microfluidic devices with high transparency (approximately 80%), has been demonstrated [11]. Moreover, this technology has also found applications in fabricating THz lenses that exhibit low absorption coefficients and stable refractive indices across a wide frequency range within the THz spectrum. By leveraging these capabilities, 3D printing holds promise for enabling advanced manufacturing processes and facilitating breakthroughs in areas like biomedicine, telecommunications, and material science [11].

3. Designing a 3D printed spiral phase plate

Designing a 3D-printed SPP involves several key considerations. Firstly, the design of the SPP needs to be carefully considered to achieve the desired vortex beam characteristics. The design should incorporate the desired azimuthal spiral phase and provide an effective conversion of the incident Gaussian beam into a vortex. To accomplish this, various techniques and materials can be utilized. For example, a common approach is to use diffractive optical elements made from materials with high transparency in the THz region.

We have used a CAD software to design the SPP with the dimensions that will be discussed in the following subsection. Once the design is finalized, the next step is to convert the CAD model into a format compatible with the 3D printer. This can be done by exporting the CAD model as an STL file, which represents the surface geometry of the object using a triangulated mesh. This STL file that will be sliced in a slicer program and converted into a GCODE file, that the 3D printer can interpret and follow to create the physical object layer by layer. Once the GCODE file is generated, it can be transferred to the 3D printer, and the printing process can begin. We have used a high-quality commercial 3D printer with high-resolution capabilities to ensure precise and accurate fabrication of the SPP. The printer used is capable of producing a single layer height of 0.2 mm for any PLA filement, providing a high level of detail and resolution in the printed object.

3.1. Calculating the step-size of the spiral phase plate

We are using a 140 GHz source in our experiment, so we can calculate the wavelengths with $\lambda = c/f$ where λ represents the wavelength, c the speed of light in a vacuum, and f the frequency. That implies that we are working with millimetre-radiation, exactly 2.1413747 mm. When light passes through the plate, its topological charge will change, in our case $l = 0$ becomes $l = 1$ or $l = 2$ respectively when the phase front of the beam is modulated into a helical shape as seen in Fig. 3.
To be able to design the SPP, we first need to consider the material we will use to print it. We will use PLA as it is a widely available type of filament and has already been characterized in the GHz and THz range. The refractive index of this filament in those ranges is 1.6 in a horizontal printing orientation [12].

We can finally calculate the step-height of the SPP using the formula mentioned in subsection 2.7, ($h = l\,\lambda/\Delta n$), where Δn stands for the difference in refractive indices that normalizes the product of the wavelength and the new topological charge of the beam. Plugging in all numbers into our formula, we get 3.568958 mm for $l = 1$ and 7.1379157 mm for $l = 2$ respectively. We then round these numbers down to the next integer multiple of the height of a 3D-printed layer.

The distinct incremental steps visible in the 3D representation of the SPP, as depicted in Fig. 5, are a consequence of the discrete layer height characteristic of traditional Fused Deposition Modeling (FDM) 3D printing process.

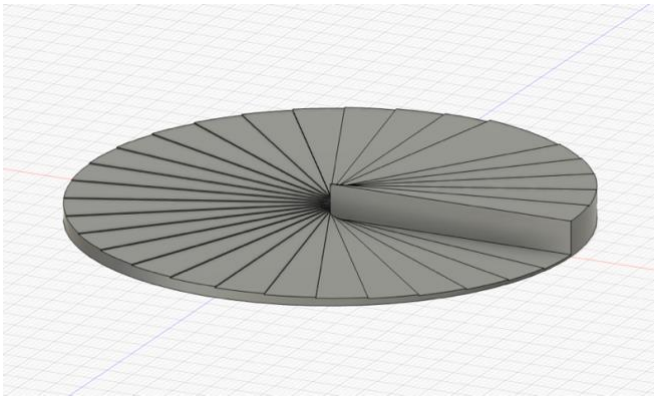

Figure 5: 3D design of the SPP used for experiments

4. Functional design of the experiment

The experiment was tailored to a continuous wave imaging setup originally designed by a previous researcher in the solid-state physics department. The square wave from the Voltcraft® 632FG oscilloscope is used to modulate the continuous THz wave from the TeraSense 140 GHz source so that the signal can be selectively amplified by "lock-in detection". The height of the source was adjusted to match that of the detector. A lens with a focal length of 120 mm produced a cylindrical collimated beam with an even wavefront, while another lens with the same focal length refocused the beam into its smallest size within the plane of detection.

Additionally, a carbonized foam material acted as a shield to minimize any potential diffractive interference effects on the beam. The previously described arrangement is depicted in the accompanying images Figs. 6. and 7.

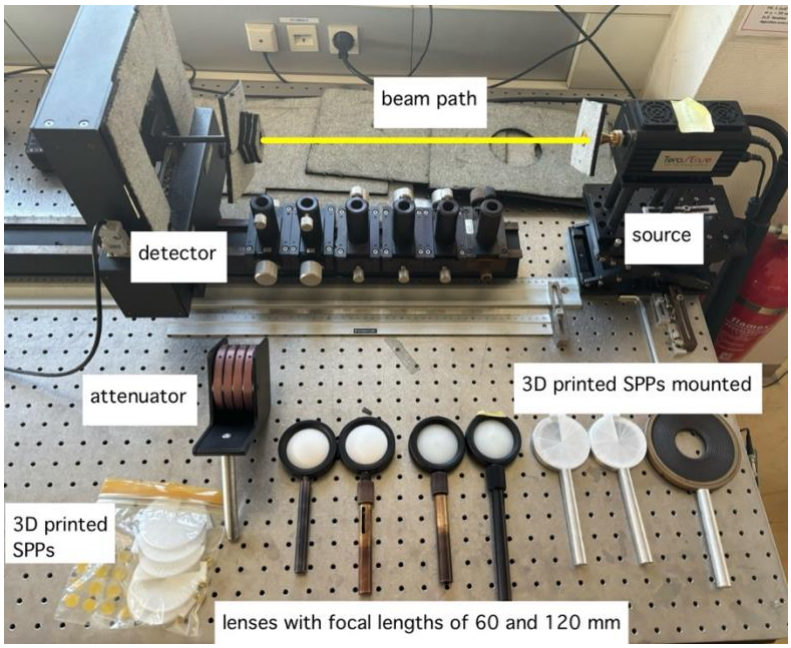

Figure 6: Picture of the experimental setup including labels of the items used

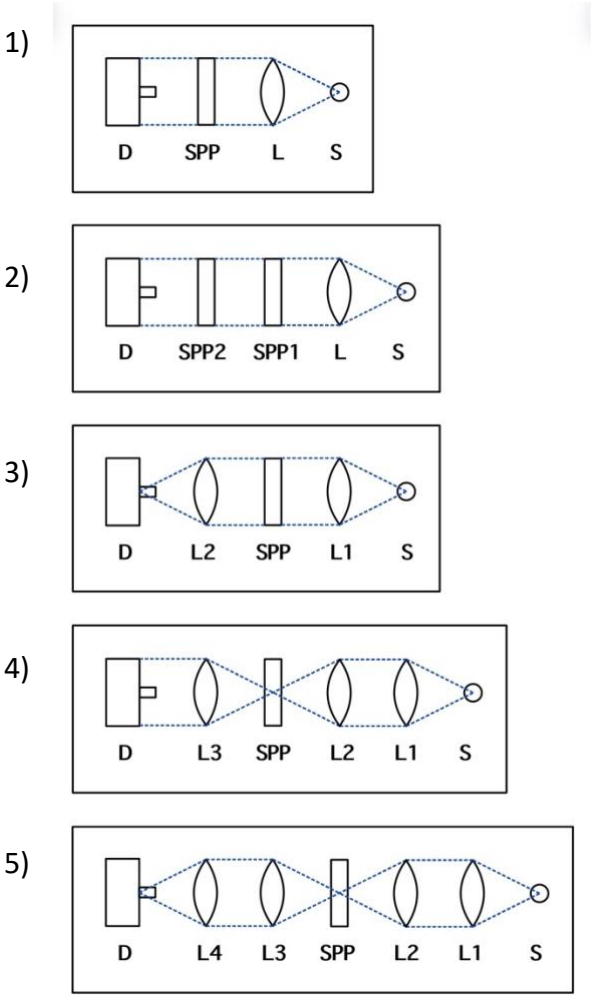

Figure 7: Schematic representations of the experiment designs. D stands for detector, SPP for spiral phase plate, L for lense, and S for source.

5. Experiment results and analysis

5.1. Experiment design 1)

The initial experiment (experiment no. 1) utilizing a first order SPP, depicted in Fig. 7, produced an anticipated nearly circular shape with a distinct singularity at the center, as shown in Fig. 8. This outcome aligns with our expectations outlined in subsection 2.7.

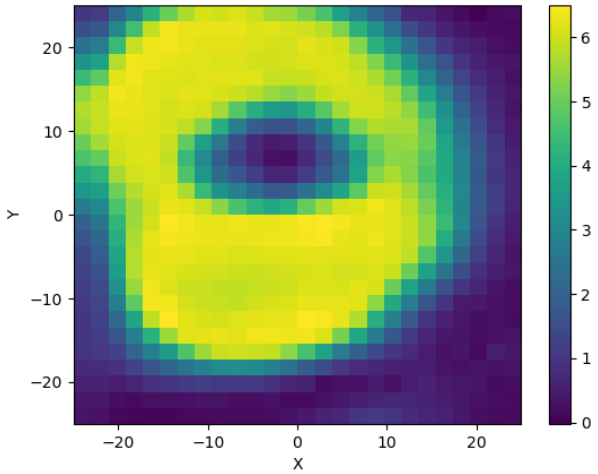

Figure 8: Measured intensities in volts over the surface of the detector for setup 1) using a 1st order SPP

Our findings were similarly promising for the experiment in the same design but using a second order SPP as shown on Fig. 9. While ideal results would display two concentric circles, our observed shape may have been influenced by unwanted diffractions, imperfect optical alignment and potential imperfections in the 3D printed SPP. Nevertheless, we can still discern the intended central point of higher intensity along with an enclosing circle of zero intensity and another outer ring exhibiting greater intensities.

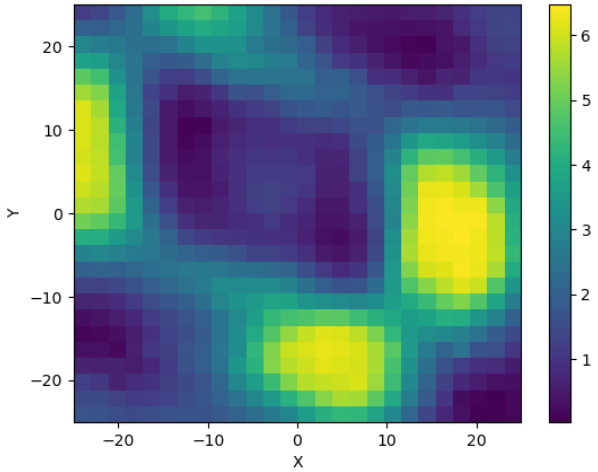

Figure 9: Measured intensities in volts over the surface of the detector for setup 1) using a 2nd order SPP

5.2. Experiment design 2)

In our second experimental configuration we attempted to reverse the effect of the SPP by introducing a second one immediately afterwards, essentially unwinding the vortex after creating it. We repeated this process with two variations: using an additional SPP with the same handedness and direction, then trying it in the opposite direction. We also tested using two SPPs with different handedness.

According to Fig. 10, adding a second SPP of matching handedness and direction did not negate the vortex effect of the initial SPP. The singularity persisted, just appearing in a slightly different shape, likely due to the additional spin imparted by the second SPP instead of converting it back into a planar wave.

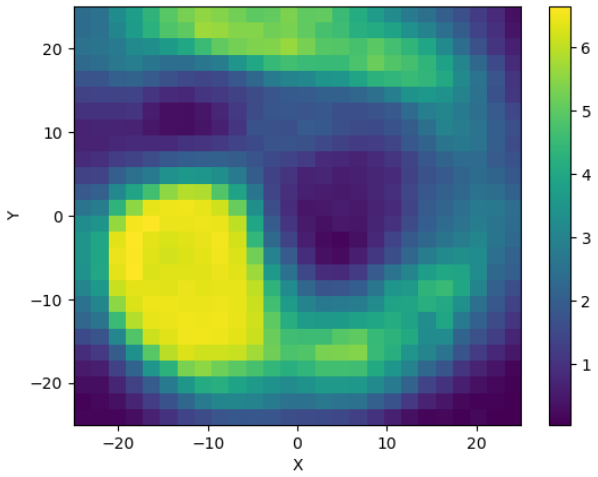

Figure 10: Measured intensities in volts over the surface of the detector for setup 2) using a two 1st order SPPs of the same handedness in a row facing the same direction

Fig. 11 demonstrates that employing a second SPP oriented in the opposite direction to the first one successfully reversed the vortex of the wavefront as anticipated, resulting in a collimated beam similar to our control measurements. The beam experienced some scattering as it passed through the SPPs before reaching the detector plane, causing it to not be entirely collimated.

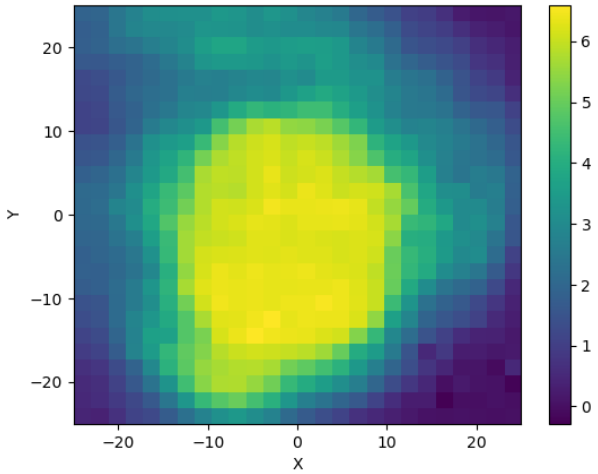

Figure 11: Measured intensities in volts over the surface of the detector for setup 2) using a two 1st order SPPs of the same handedness in a row facing the opposite direction

Furthermore, when using a second SPP with opposite handedness in our setup, it led to complete scattering of the beam as shown on Fig. 12. In this scenario, an already spiral incident wave at the second SPP gets twisted in the opposite direction, leading to an exiting beam without a distinct phase and likely containing a combination of both left- and right-handed vortices with inefficient conversion. Those conflicting chiralities either nullify each other or cause significant dispersion, thus producing this outcome.

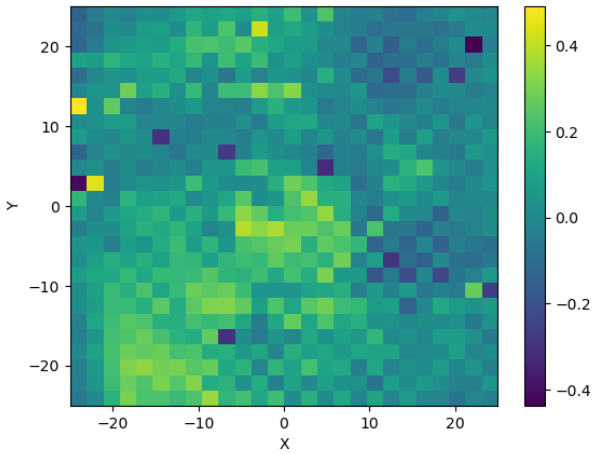

Figure 12: Measured intensities in volts over the surface of the detector for setup 2) using a two 1st order SPPs of different handedness in a row facing the same direction

5.3. Experiment design 3)

In our third experiment setup, we positioned a SPP between two lenses with identical focal lengths to investigate the effect of refocusing the spiralized beam on the plane of the detector.

Fig. 13 does not demonstrate a distinct singularity or a sufficiently small, refocused beam. This may be attributable to imprecise positioning of the second lens and the detector, as well as a resolution that is not finely tuned to resolve the central singularity.

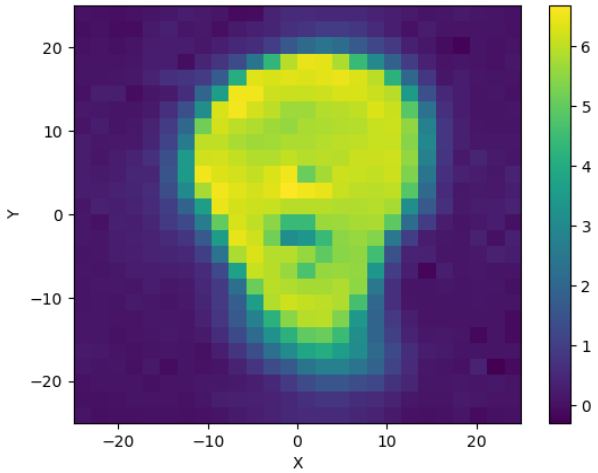

Figure 13: Measured intensities in volts over the surface of the detector for setup 3) using a 1st order SPP

Additionally, in this configuration, the assumption of using a collimated beam for the last lens to accurately focus onto the image plane may not hold true. The presence of the SPP and the long path from the source to the last lens may result in a beam that is not well collimated at this point, hence reducing the effectiveness of the last lens. Any displacement in focal length caused by the incident spiral wave could further contribute to dispersion issues with previous the lenses and SPP, ultimately affecting the observed beam shape. Consequently, it can be inferred that this setup is not suitable for precise imaging purposes.

5.4. Experiment design 4)

In our fourth experiment setup we placed the SPP after 2 lenses, which collimate and then refocus the light beam in the plane of the SPP. Subsequently, another lens is used to recollimate the beam before it reaches the detector. The objective was to observe if a helical structure could be generated while focusing the beam at a point.

Using a first order SPP did produce a small but noticeable singularity as depicted in Fig. 14. Indicating a helical beam. In this case, to counteract saturation issues caused by elevated amplitudes resulting from beam refocusing, an attenuator with 10% transparency was placed between these lenses, resulting in notably lower voltage compared to previous experiments. This suggests that our order 1 SPP also functions effectively with focused light beams.

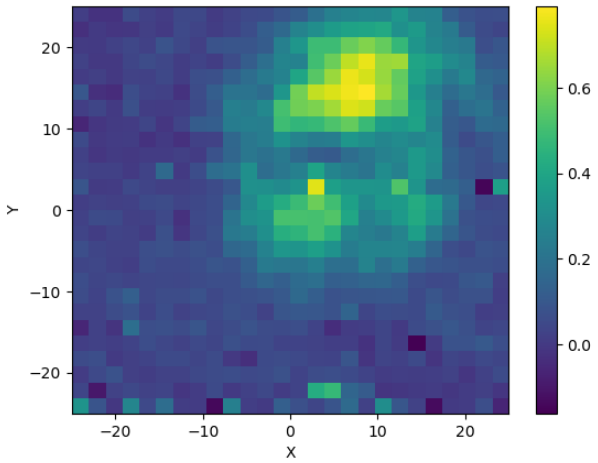

Figure 14: Measured intensities in volts over the surface of the detector for setup 4) using a 1st order SPP, 2 lenses with 120 mm focal length, and a 3rd with 60 mm

We also attempted a similar setup using identical lenses, but with an order 2 SPP as depicted in Fig. 15. However, this did not yield clear concentric circles as anticipated. This discrepancy may stem from complexities within the phase front created by the order 2 SPP.

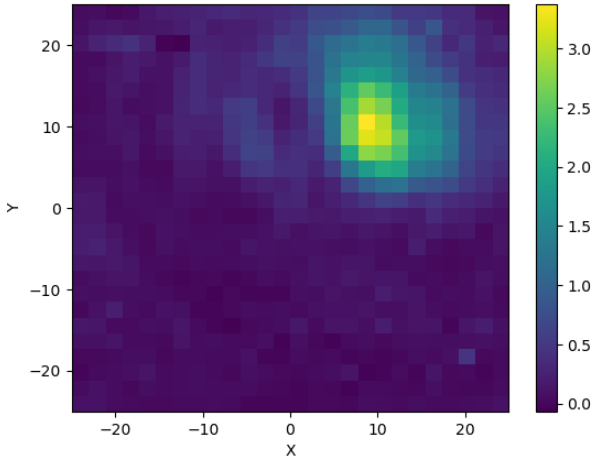

Figure 15: Measured intensities in volts over the surface of the detector for setup 4) using a 2nd order SPP, 2 lenses with 120 mm focal length, and a 3rd with 60 mm

5.5. Experiment design 5)

In our fifth and final experimental setup, we began with the previous configuration but included an additional 4th lens before the detector in order to once again focus the beam on the plane of the detector.

The utilization of the first order SPP effectively produced the spiral phase front depicted in Fig. 16. The singularity is distinctly observable, although it is noteworthy that the beam, similar to our experimental setup in subsection 5.3., has not been sufficiently refocused.

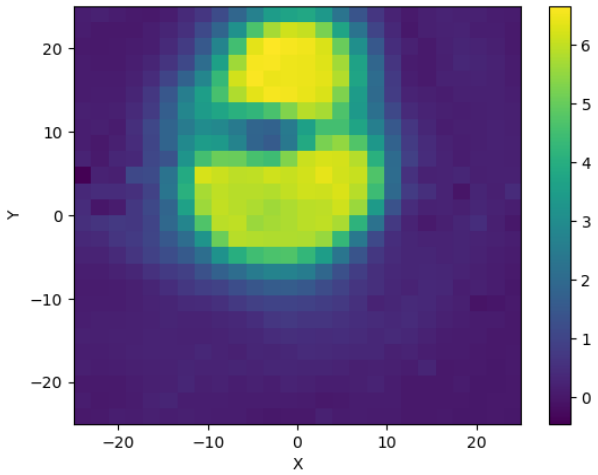

Figure 16: Measured intensities in volts over the surface of the detector for setup 5) using a 1st order SPP, 2 lenses with 120 mm focal length, and an other 2 with 60 mm

When swapping the SPP out to a second order one in the same setup, we were not able to produce the anticipated concentric circles as seen on Fig. 17., just as discussed in subsection 5.4. in our 4th experimental setup.

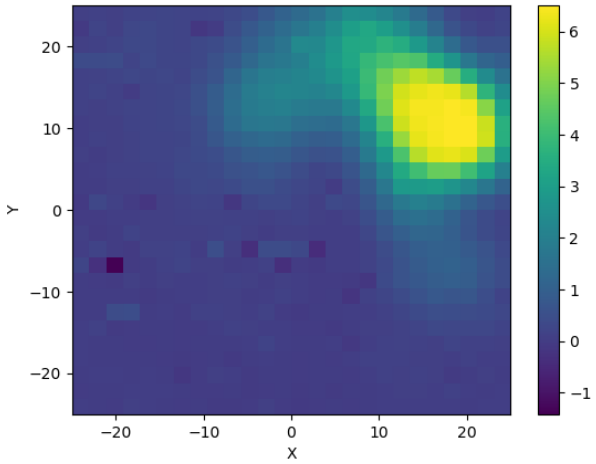

Figure 17: Measured intensities in volts over the surface of the detector for setup 5) using a 2nd order SPP, 2 lenses with 120 mm focal length, and an other 2 with 60 mm

6. Summary and outlook

The aim of the conducted experiments detailed in this thesis was to explore the influence of SPPs on light wavefronts, particularly concerning the use of helical beams for spectroscopic purposes. Our experimentation featuring different arrangements of SPPs, and optical elements has resulted in valuable insights into generating and controlling helical beams, and their potential use in spectroscopy.

Circularly polarized light carries orbital angular momentum due to its azimuthal phase dependence of $e^{il\varphi}$, leading to a helical phase front instead of a planar one as depicted in Fig. 3. This alteration in the phase front can be generated using various methods. Here we explored its generation using SPPs, that introduce a phase delay that varies with the azimuth angle. This is achieved by varying the thickness of the plate radially. These SPPs can be readily produced utilizing a commercially accessible 3D printer.

During the design phase of the SPPs, it was crucial to appropriately adjust the calculated step height to align with the layer height of the 3D printer being used. Due to their smaller size, these optical elements had a relatively short printing time of approximately 15 minutes when produced on a 3D printer with a maximum speed of 250 mm/s. However, special attention was required for the first layer due to residual PLA that could be dragged by the nozzle. Even small amounts of extra material could result in imperfections in the optical element, reducing its efficiency or causing additional scattering of light. Despite these minor considerations, newer 3D printers make this printing process relatively straightforward and require minimal additional oversight.

In our first experimental configuration we demonstrated the simplest way to form and image using a THz vortex beam, providing evidence for our concept and validating the effectiveness of both SPPs, although this configuration is not very suitable for spectroscopic purposes. In our second setup we were able to successfully refocus the helical beam despite encountering challenges with the non-planar incident wave front.

The fifth setup was crucial for spectroscopic purposes, yielding excellent results with the first order SPP. It is essential to consider the phase of the propagating beam, particularly when using optical elements designed for planar incident waves. Unwrapping vortex beams may also be necessary to optimize control of the beam through spectrometer optics after it interacts with a sample. The correct orientation of the second "unwrapping" SSP, as depicted in Fig. 11 above, is important in this case.

Our results indicate several potential areas for future investigation and expanded research, despite our primary focus being on duplicating existing studies rather than revealing novel findings. Some of the promising future areas of research include spectroscopy, imaging, communication, and even medical applications.

Addressing the challenges in precise optical alignment is essential for enhancing the accuracy and consistency of future experiments. Further insight into controlling light waves can be gained by investigating even higher order SPPs, different materials, or alternative phase plate arrangements. The generation of helical beams using SPPs holds potential to benefit practical applications like optical communication and imaging, contributing to the advancement of knowledge and continued development. Utilizing theoretical models and simulation tools is valuable for predicting and analyzing the behavior of light waves in complex optical systems, improving understanding to guide future experimentation.

7. Table of figures

8. Bibliography

[1] H. A. Hafez, X. Chai, A. Ibrahim, S. Mondal, D. Férachou, X. Ropagnol and T. Ozaki, "Intense terahertz radiation and their applications," *Journal of Optics,* vol. 18, 2016.

[2] K. Nallappan, H. Guerboukha, M. Seghilani, T. Ma, J. Azaña, C. Nerguizian and M. Skorobogatiy, "Multiplexing of terahertz wireless communication channels using vortex beams," in *2017 42nd International Conference on Infrared, Millimeter, and Terahertz Waves (IRMMW-THz)*, Cancun, Mexico, 2017.

[3] S. Zhong, "Progress in terahertz nondestructive testing: A review," *Frontiers of Mechanical Engineering,* vol. 14, pp. 273-281, 2019.

[4] V. E. Rogalin, I. A. Kaplunov and G. I. Kropotov, "Frontiers of Mechanical Engineering," *Optics and Spectroscopy,* vol. 125, pp. 1053--1064, 2018.

[5] I. Echchgadda, J. E. Grundt, C. Z. Cerna, C. C. Roth, J. A. Payne, B. L. Ibey and G. J. Wilmink, "Terahertz Radiation: A Non-contact Tool for the Selective Stimulation of Biological Responses in Human Cells," *IEEE TRANSACTIONS ON TERAHERTZ SCIENCE AND TECHNOLOGY,* vol. 6, pp. 1-15, 2016.

[6] D. N. Khiabani, "All About Circuits," 2019. [Online]. Available: https://www.allaboutcircuits.com/technical-articles/introduction-to-terahertz/. [Accessed 08 2023].

[7] W. Demtröder, Experimentalphysik 2, Kaiserslautern: Springer Spektrum, 2012, pp. 194-195.

[8] P. Coullet, L. Gil and F. Rocca, "Optical vortices," *Optics Communication,* vol. 73, pp. 403-408, 1 November 1989.

[9] X. Wang, Z. Nie, Y. Liang, J. Wang, T. Li and B. Jia, "Recent advances on optical vortex generation," *Nanophotonics,* vol. 7, pp. 1533-1556, 2018.

[10] A. M. Yao and M. J. Padgett, "Orbital angular momentum: origins, behavior and applications," *Advances in Optics abd Photonics,* vol. 3, pp. 161-204, 2011.

[11] H. Wang, Q. Song, Y. Cai, Q. Lin, X. Lu, H. Shangguan, Y. Ai and S. Xu, "Recent advances in generation of terahertz vortex beams and their applications," *Chinese Physics B,* vol. 29, p. 097404, 2020.

[12] T. D. Ngo, A. Kashani, G. Imbalzano, K. T. Nguyen and D. Hui, "Additive manufacturing (3D printing): A review of materials, methods, applications and challenges," *Composites Part B: Engineering,* vol. 143, pp. 172-196, 2018.

[13] K. G. K. Monia, C. G. Jones, S. K. Sharifi and C. Chen, "3D-Printed Microfluidic Devices for Enhanced Online Sampling and Direct Optical Measurements," *ACS Sensors,* vol. 5, no. 7, p. 2044–2051, 2020.

[14] A. T. Clark, L. B. Kong, J. F. Federici and I. Gatley, "Effect of 3D Printing Parameters on the Refractive Index, Attenuation Coefficient, and Birefringence of Plastics in Terahertz Range," *Advances in Materials Science and Engineering,* vol. 2021, pp. 1-9, 2021.

[15] P. Senthilkumaran, Singularities in Physics and Engineering, Bristol: IOP Publishing Ltd , 2018.

[16] Z. Zhang, X. Wei, C. Liu, K. Wang, J. Liu and Z. Yang, "Rapid fabrication of terahertz lens via three-dimensional printing technology," *Chinese Optics Letters,* vol. 13, no. 2, pp. 022201--022201, 2015.